Astron. Astrophys. 348, 98–112 (1999)

ASTRONOMY AND ASTROPHYSICS

The new Basel high-latitude field star survey of the Galaxy

II. The thick disk component: density structure, luminosity function, and metallicity distribution

Roland Buser[1], **Jianxiang Rong**[2], **and Salih Karaali**[3]

[1] Astronomisches Institut der Universität Basel, Venusstr. 7, CH-4102 Binningen, Switzerland
[2] Astronomy Department, Nanjing University, Nanjing 210008, P.R. China
[3] Istanbul University Science Faculty, Department of Astronomy and Space Sciences, 34452 University – Istanbul, Turkey

Received 29 December 1998 / Accepted 19 May 1999

Abstract. We present an expanded and refined analysis of the Galactic thick disk as observed in seven fields of the new Basel RGU star count and color survey data. Based on the optimized structural models which were obtained in the initial analysis (Buser et al. 1998a, hereafter Paper I), we now employ the same systematic least-squares algorithm, introducing more realistic luminosity functions for each population component, applying a more adequate matrix of color transformations in simulating the data, and extending the structural parameter ranges in order to determine improved characteristics of the thick-disk model.

Compared with the earlier results of Paper I, the present models provide χ^2-fits to the data which are improved by about 25%. From these we conclude that, on the one hand, each of the thin disk, thick disk, and halo components has its own local luminosity function, characterized by a distinctly specific shape and metallicity. On the other hand, the above improvement also allows us to derive more reliable estimates of optimized parameter values and constraints for the structural thick-disk model. According to our currently best models, we find the Galactic thick disk to have local density $\bar{n}_1 = 5.9 \pm 3\%$ of the local thin-disk density, exponential scale length $\bar{d}_3 = 3.0 \pm 1.5$ kpc, and exponential scale height $\bar{h}_4 = 0.91 \pm 0.3$ kpc. We also confirm the result of Paper I that the data are consistent with a metallicity distribution of the thick disk centered on $\langle [M/H] \rangle \sim -0.63$ dex and having dispersion $\sigma_{\langle [M/H] \rangle} \sim 0.4$ dex.

While these results are in remarkable agreement with the majority of independent recent determinations of the global properties of the Galactic thick disk, we cannot yet exclude the possibility that the sizeable dispersions associated with the mean parameter values are indicative of structural differences between the individual fields that may largely be due to features of the real thick disk – reflecting intrinsic deviations from the smooth physical entity described by the model. Still, pending the analysis of the second catalog of homogeneous RGU data in seven additional directions, the present data marginally favor an accretion model of the origin of the thick disk as a major episode in the merger history of formation of the larger Galaxy.

Send offprint requests to: Roland Buser (buser1@ubaclu.unibas.ch)

Key words: surveys – Galaxy: abundances – Galaxy: fundamental parameters – Galaxy: structure

1. Introduction

The new Basel RGU high-latitude survey provides a three-color data base which is suitable for the determination of the larger-scale density and metallicity distributions of the major stellar population components of the Milky Way Galaxy. In Paper I, we have developed a least-squares algorithm for the statistical analysis of the data in terms of four-component parameterized Galactic models including a young and an old exponential thin disk, an exponential thick disk, and an oblate spheroidal halo component. Using the available photometric G and G-R star count and color data, the algorithm has been extensively tested by deriving optimized parameter values for both individual fields and the combined survey of seven fields through systematic exploration of parameter space. These preliminary test results have shown the data to be highly homogeneous and describable by a global model of the Galaxy whose structural parameter values are in general agreement with the canonical literature. Finally, we have shown that, based on the structural model thus derived, it is possible in principle to exploit the metallicity-sensitive U-G data for determining the larger-scale metallicity distribution of the Galactic thick disk as well.

In practice, however, failure of our initial attempt to prove or disprove in our data the existence of a metallicity gradient of the thick disk – which is crucial for discriminating between possible formation scenarios of this component – soon convinced us that our exploration and control of the structural models in general and of the metallicity effects in particular need to be advanced to significantly higher levels for a successful match to the quality of the available data.

Thus in this paper, we reexamine and upgrade our preliminary model (Buser & Rong 1995, 1996a,b, and Paper I) by extending the analysis (1) beyond the critical structural parameter ranges found so far, (2) to include more recent data on the component-specific luminosity functions, and (3) to account for

improved photometric transformations used in calculating star counts and color distributions. In Sect. 2, we provide a more detailed discussion of the thick-disk local density and structural parameter values resulting from the model calculations described in Paper I. In particular, we show that models including only a weak (or even zero) thick-disk component can be plainly ruled out by the present data. However, we also show that the variation ranges of the thick-disk parameters explored in Paper I must be expanded in order to better account for field-to-field variations in the observed star counts and color distributions and to improve the determination of optimized parameter values and constraints. To this same end, we also describe new model calculations implementing (1) new input for the luminosity functions as derived from HIPPARCOS and from globular cluster data, and (2) more adequate UBV-RGU transformations for the red stars. In Sect. 3, results obtained from the χ^2-analysis of these new model calculations are presented, and optimized thick-disk parameters hence derived are briefly discussed. In Sect. 4, we compare these results to other work and summarize our main conclusions. Finally, we briefly mention the prospects for future work on this survey project.

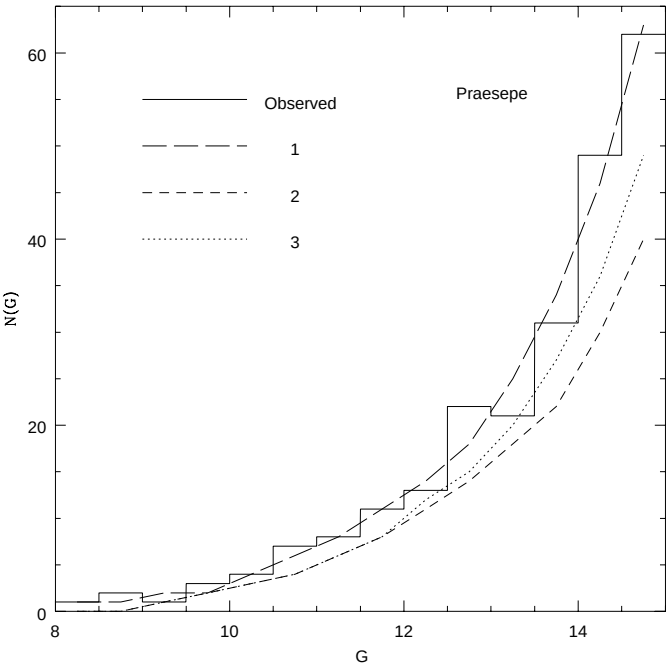

Fig. 1. Star counts for the Praesepe field. The calculated curves are for the field-specific optimized model with (1) $n_1 = 0.068$ and for lowest-χ^2 models having (2) $n_1 = 0.0$, (3) $n_1 = 0.02$.

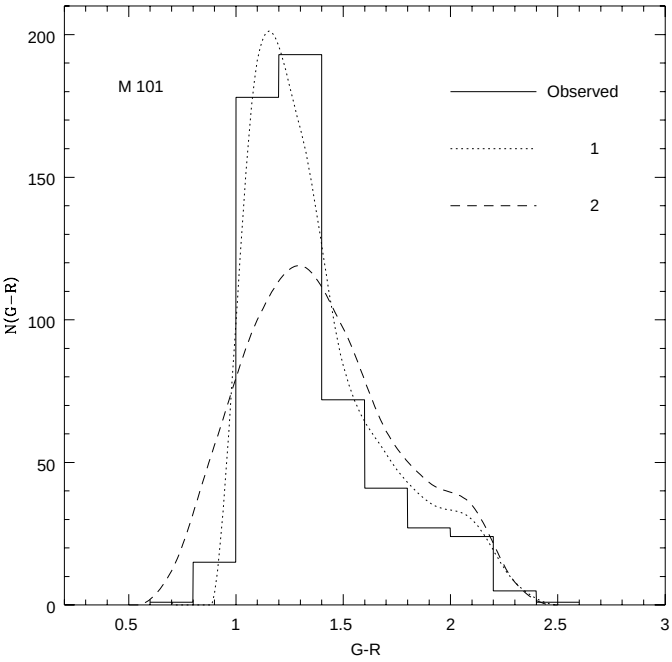

Fig. 2. $G - R$ color distribution for the field M101. The calculated curves are for the field-specific optimized model with (1) $n_1 = 0.065$ and for the lowest-χ^2 model having (2) $n_1 = 0.0$.

2. Analysis of thick-disk parameters

The purpose of this section is twofold. First, we shall demonstrate that the thick-disk component in our Galactic models is indispensable for explaining the observed star count and color data. And secondly, we shall show that our preliminary knowledge of the thick-disk parameters (as essentially derived in Paper I) can still be made more reliable by allowing for wider ranges of thick-disk parameters and by improving on basic model input data and photometric calibration.

2.1. Evidence for the thick-disk component

Evidence for the presence of a substantial thick-disk component in the new Basel survey data is most prominently illustrated in Figs. 1 and 2. They show how the lowest-χ^2 models, calculated with or without a thick-disk component, differ dramatically in their performances of matching the star counts and stellar distributions as functions of apparent G magnitude and G-R color observed in the two fields Praesepe and M101, respectively. These differences correspond to factors larger than 1.5 and up to 2.5 in χ^2_{min}-values, clearly indicating that, if acceptable models without a thick disk could be found at all, they would have to have structural parameter values for the thin disk and halo ranging far beyond the adopted canonical limits. This conclusion is corroborated by the results given in Table 1, which summarizes a sample of representative calculations of lowest-χ^2 models for three different assumed values of the local thick-disk density, n_1, including the optimized value from Paper I (model A) and a model with zero thick disk (model B). For models with no thick disk at all (i.e., $n_1 = 0.00$) or with only a weak thick disk (i.e., $n_1 = 0.01$), both the χ^2-values and their minima, $\chi^2_{min,B\vee C}$, become excessively large; in fact, as given by $N_A(\chi^2 < \chi^2_{min,B\vee C})$ in the last column of Table 1, in all cases there are several hundred up to a few thousand(!) models A (i.e., including a strong thick disk) which have χ^2-values less than χ^2_{min} obtained for models B or C (i.e., including a zero thick disk or only a weak thick disk.)

Table 1 also shows that for the best (i.e., χ^2_{min}) models B and C, the scale height of the old thin-disk dwarfs, h_1, and the local density of the halo, n_2, both increase significantly above their optimized values found for model A in Paper I, to compensate for the missing thick-disk stars.

Thus, models with only a weak or even a zero thick disk are plainly ruled out by the present results. The evidence provided here (and in Paper I) leaves no doubt that a substantial thick-disk component exists in the Milky Way Galaxy with a local density (relative to the thin disk) $n_1 > 0.02$.

2.2. Thick-disk parameters and constraints

We now examine in greater detail each of the three thick-disk parameters included in our models. For this purpose, we use the same procedure as applied in Paper I for determining their optimized values by calculation of the χ^2-curves and the frequency distributions of parameter values for low-χ^2 models. Note that the χ^2-curves have been calculated to show how χ^2 changes upon variation of a particular parameter throughout its adopted range, while *all* other parameters (i.e., including the two remaining thick-disk parameters) are fixed at their values found for the globally best-fitting model identified by $\chi^2_{1,s,min}$ in Paper I.

2.2.1. Local density

Figs. 3 and 4 are representative illustrations – i.e., calculated for the combined survey of seven fields – of the general properties and behavior of the χ^2-curves and the frequency distributions for the local density of the thick disk. Good models, i.e., with $\chi^2 \leq 1.1\chi^2_{1,s,min}$, all have $n_1 > 0.02$! Even for the adopted quality limit, $\chi^2 \leq 1.5\chi^2_{1,s,min}$, only 3.8% and 12.4%, respectively, of the models are found to have $n_1 = 0$, for just two (M67 and SA 141) out of all seven fields. (Incidentally, these two fields are those which provide the lowest counts (~ 750) by far of all seven survey fields analysed here.) However, with ξ increasing from 1.1 to 1.5, the frequency distributions tend to become wider-ranged, with their peaks shifting from $n_1 \sim 0.06$ to $n_1 \sim 0.03$, indicating that the constraint on this parameter derived in Paper I ($\sigma_{\bar{n}_1} = 0.015$) may in fact be weaker. This will indeed be confirmed by the extended analysis below.

Thus, from the frequency distributions of Fig. 4, we cannot either exclude that acceptable models may even exist with $n_1 > 0.07$, at least for a few of the Galactic directions investigated here. Evidence of a thick-disk with such higher local densities in the range $\sim 6-12\%$ has also previously been found from field-RHB stars (Rose 1985) and, in particular, from radial velocities (Sandage 1987), from proper motions (Casertano et al. 1990), and from combined photometric and proper motion data (Ojha et al. 1994a,b). For a more conclusive comparison with these recent independent results, we shall, therefore, have to extend the parameter range in our model calculations, which will also allow us – in Sect. 3 below – to obtain a safer upper limit or at least a more reliable constraint on the optimized mean value $\bar{n}_1$. Before taking this step, however, we shall now determine

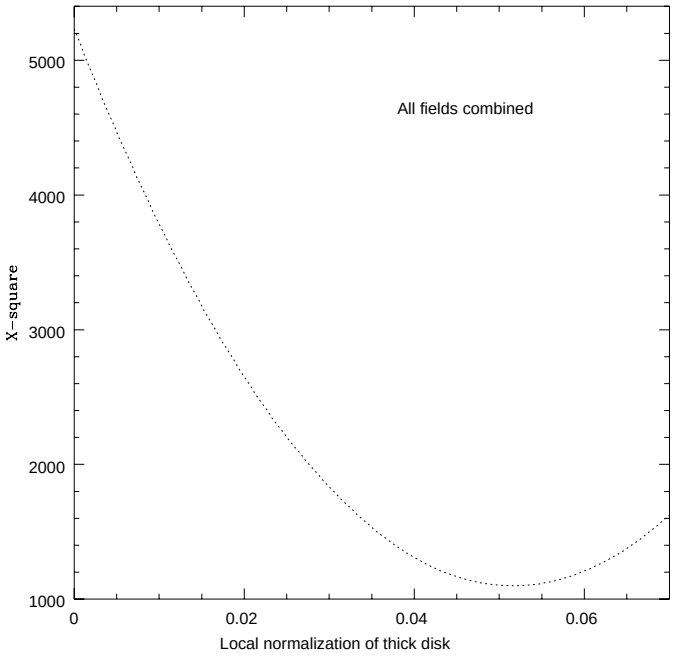

Fig. 3. χ^2-curve for the local density, n_1, of the thick disk, derived from the combined survey of seven fields and for the parameter range adopted in Paper I.

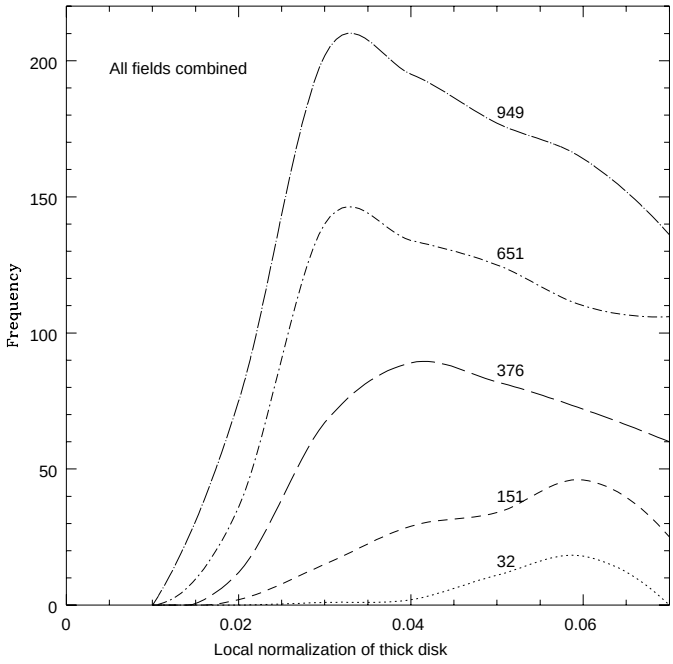

Fig. 4. Frequency distributions for the local density, n_1, of the thick disk, derived from the combined survey of seven fields and for the parameter range adopted in Paper I. The sequence of curves from bottom to top corresponds to values of ξ growing from 1.1 to 1.5; labels indicate the number of models involved.

if similar extensions of the variation ranges are required for the scale length and scale height parameters of the thick disk by examining more closely the general properties and behavior of their χ^2-curves and frequency distributions.

Table 1. Compensation of zero or weak thick disk by thin-disk and halo stars[1]

Field		χ^2_{min}			Old thin disk, h_1			Halo, n_2			$N_A(\chi^2 < \chi^2_{min,B\vee C})$	
No.	Name	A	B	C	A	B	C	A	B	C	B	C
1	Praesepe	115	241	208	1.19	1.20	1.20	0.0020	0.0021	0.0021	2331	1679
2	M 101	1032	1928	1627	0.86	1.11	1.05	0.0003	0.0014	0.0009	2637	1813
3	M 67	329	407	366	1.02	1.20	1.18	0.0014	0.0016	0.0015	1298	972
4	SA 54	472	813	553	0.80	0.98	0.89	0.0010	0.0022	0.0016	2445	507
5	SA 57	652	1309	916	0.80	1.07	0.96	0.0011	0.0018	0.0013	1129	765
6	SA 141	342	455	384	0.97	1.08	0.99	0.0023	0.0025	0.0024	587	108
7	M 5	3316	11542	7231	0.97	1.20	1.20	0.0003	0.0013	0.0009	1956	1217
1-7	Combined	1103	2606	1904	0.91	1.19	1.13	0.0005	0.0014	0.0011	2038	1544

[1] Thick-disk local densities, n_1, are assumed to be 0.054, 0.000, and 0.010 of the local thin-disk density in models A, B, and C, respectively. Model A is the globally best model from Paper I.

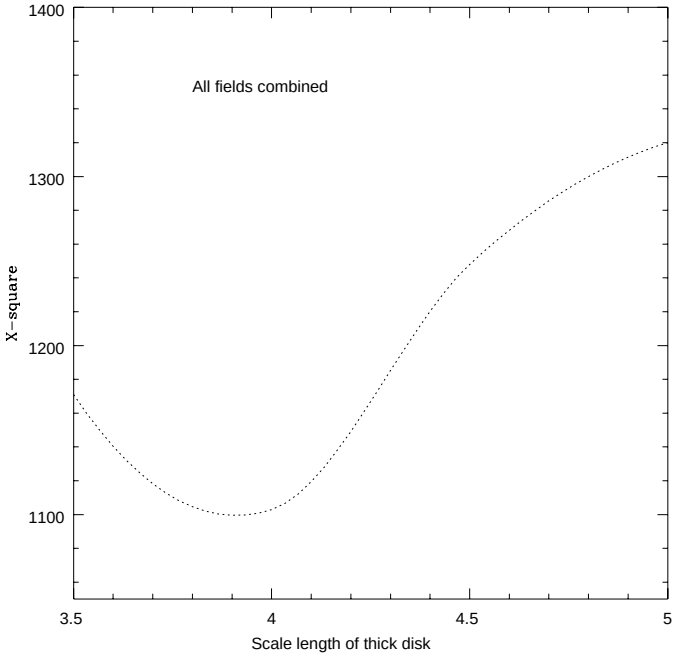

Fig. 5. χ^2-curve for the scale length, d_3, of the thick disk, derived from the combined survey of seven fields and for the parameter range adopted in Paper I.

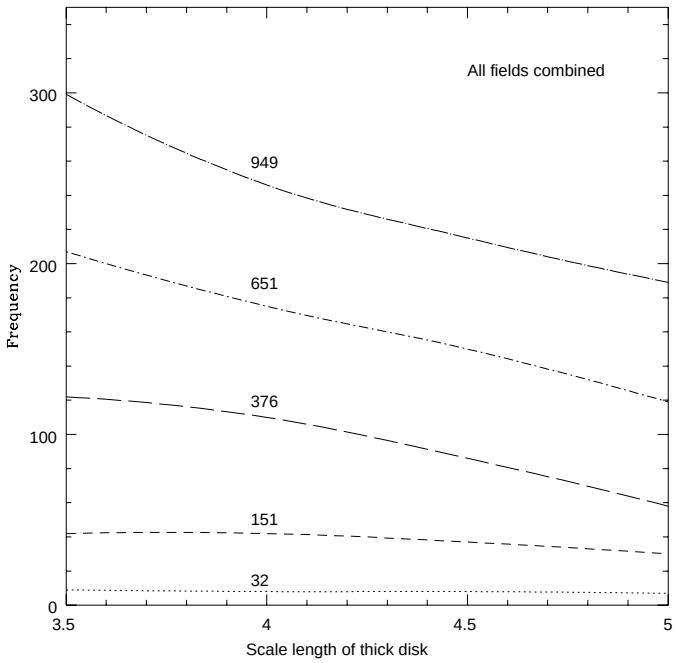

Fig. 6. Frequency distributions for the scale length, d_3, of the thick disk, derived from the combined survey of seven fields and for the parameter range adopted in Paper I. The sequence of curves from bottom to top corresponds to values of ξ growing from 1.1 to 1.5.

2.2.2. Scale length

Adopting a local density $n_1 = 0.054$, found for the thick disk from the parameter optimization calculations in Paper I, the (representative) χ^2-curve and frequency distributions for the scale length (d_3) parameter as derived from the combined survey of seven fields are shown in Figs. 5 and 6.

Due to the generally high Galactic latitudes of the survey fields, the present data are naturally expected to be rather insensitive to the scale length parameter (d_3). This is borne out by the relatively low amplitude of the χ^2-curve, $(\chi^2 - \chi^2_{min})/\chi^2_{min} < 0.1$, within most of the variation range in Fig. 5, and by the very flat frequency distributions for the good models ($\xi \leq 1.2$) in Fig. 6. These results for the combined survey are very similar to those obtained for each individual field. In Paper I, a correspondingly weak constraint, $\sigma_{\bar{d}_3} = 1.0$ kpc, on the optimized value $\bar{d}_3 = 4.25$ kpc was derived for this parameter. The accuracy of this value is rather low, however, because the position of $\chi^2_{min}(d_3)$ in Fig. 5 and the resulting $\bar{d}_3 = 4.25$ turned out to be close to the lower limit of the variation range (3.5 kpc), and uniform extrapolations of the χ^2- and the frequency distribution curves beyond the above limit at $d_3 < 3.5$ kpc had to be assumed in estimating the constraint. Obviously, further calculations are required now to confirm (or reject) this assumption and to derive more reliable optimized values for this parameter and its constraints.

2.2.3. Scale height

On the other hand, the χ^2-curves and, particularly, the frequency distributions for the thick-disk scale height (h_4) are not simi-

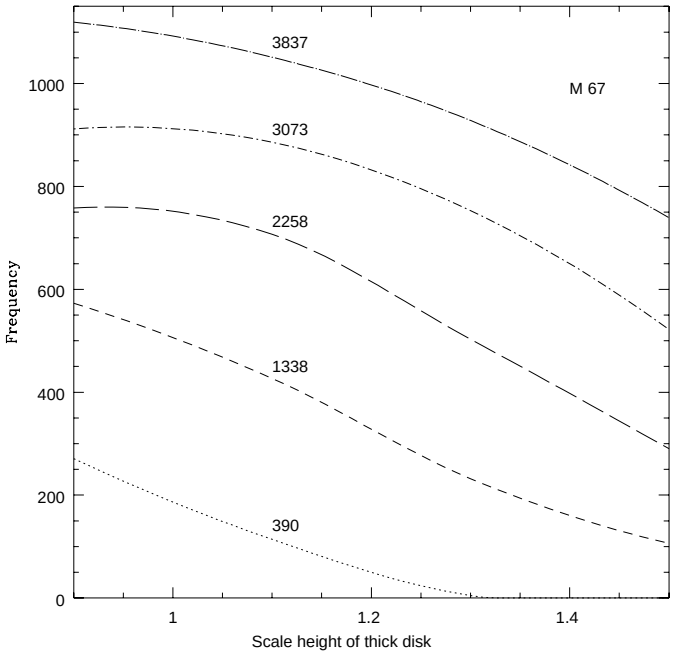

Fig. 7. Frequency distributions for the scale height, h_4, of the thick disk, derived for the field M67 and for the parameter range adopted in Paper I. The sequence of curves from bottom to top corresponds to values of ξ growing from 1.1 to 1.5.

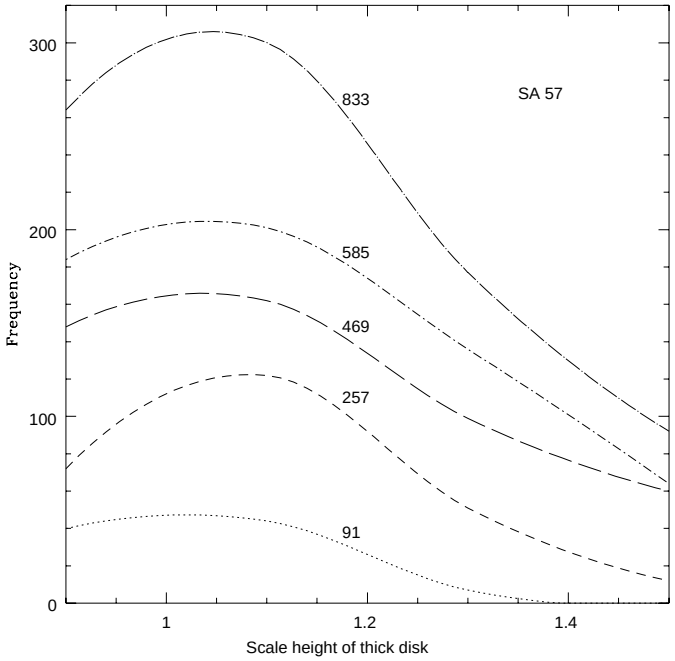

Fig. 8. Frequency distributions for the scale height, h_4, of the thick disk, derived for the field SA57 and for the parameter range adopted in Paper I. The sequence of curves from bottom to top corresponds to values of ξ growing from 1.1 to 1.5.

larly uniform among the individual fields, as they are for the scale length. Although all the individual values of χ^2_{min} occur at scale heights $h_4 > 1.0$ kpc, the actual χ^2-curves depend sensitively on the Galactic direction, the count completeness

Table 2. Extended variation ranges of thick-disk density law parameters

Parameter	Symbol	Unit[1]	Old range (Paper I)	New range adopted here
local density	n_1	n_0	0.00 – 0.07	0.00 – 0.11
scale length	d_3	kpc	3.5 – 5.0	2.5 – 6.0
scale height	h_4	kpc	0.9 – 1.5	0.3 – 1.7

[1] $n_0 = 0.078$ stars/pc^3 is the optimized value found in Paper I for the local density of the old thin disk, while the new optimized value derived below is $n_0 = 0.11$ stars/pc^3 (see the text).

magnitude limit, and the correspondingly different star counts in each field, leading to very different χ^2-growth rates as functions of h_4. Thus, for a slow χ^2-growth rate, acceptably good models satisfying $\chi^2 \leq \chi^2_{max} \leq 1.2 \times \chi^2_{min}$ may still be found far from the parameter value characterizing the actual χ^2_{min}, and even at (or beyond) the lower boundary (0.9 kpc) of the adopted variation range of h_4.

This case is illustrated in Fig. 7, where we show the frequency distribution for the scale height of the thick disk, h_4, derived from the data in the field near M67 (i.e., in the outer Galaxy at $l = 210°, b = 32°$). Obviously, the most frequent value occurring among the best models (dotted and short-dashed curves in lower part of figure) is $h_4 = 0.9$ kpc, and a clear trend to the same also persists with the lower-quality models ($\xi \geq 1.3$). Thus, even though the weighted mean, or optimized, value $\bar{h}_{4,M67} = 0.96$ kpc determined for this individual field in Paper I is still well within $2\sigma_{\bar{h}_{4,all}} = 0.30$ kpc of the optimized parameter value, $\bar{h}_{4,all} = 1.15$ kpc, derived from the all-field survey, it is also evident from the present data that the best results for an individual field like M67 should very likely be obtained from models having a thick-disk scale height $h_4 \leq 0.9$ kpc.

This conclusion also holds for at least three other fields of the present survey (M101, Praesepe, and SA141), whose frequency distributions exhibit essentially the same behavior as the M67 field discussed above, providing strong indications that the thick-disk scale height is lower than suggested by the preliminary results derived in Paper I. On the other hand, the frequency distributions for the fields SA54 and M5 are similar to that shown in Fig. 8 for the polar field SA57, with best-model curves ($\xi = 1.1 \vee 1.2$) having flat but well defined peaks at $\sim 1.0 \leq h_4 \leq 1.2$ and which become significantly more strongly pronounced at $\xi \geq 1.3$.

To summarize, Figs. 5-8 tell us that, in order to derive more reliable optimized parameter values and constraints for both individual fields and the all-survey data, we have to extend our analysis beyond the variation limits adopted originally for the thick-disk parameter ranges. Hence, new model calculations will be carried out according to Table 2.

2.3. Luminosity functions and photometric transformations

Of course, the structural parameter values derived from the new Basel data critically depend on the reliability of basic model input and calibration data. In the first place, these are given by the

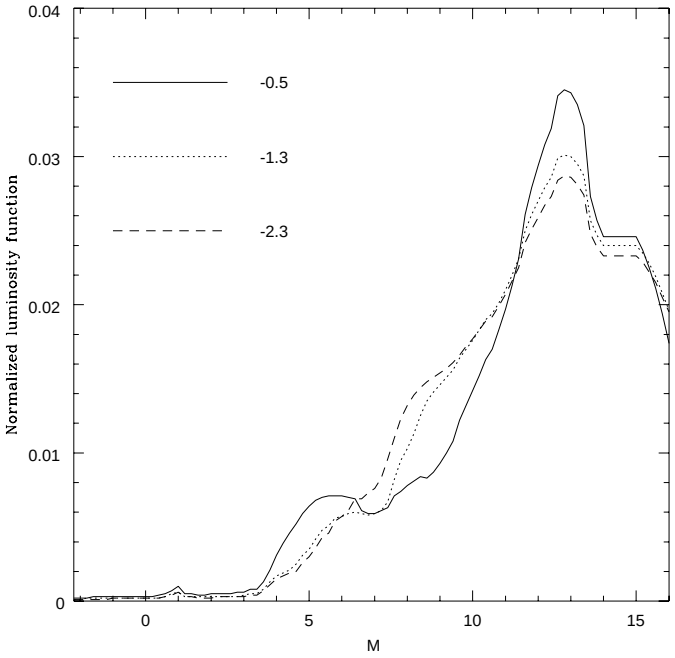

Fig. 9. Normalized luminosity functions for metal-poor populations. They were taken from the globular-cluster luminosity functions published by McClure et al (1986) for $4^m \leq M_V \leq 9^m$ primarily to provide a possibly more adequate representation of the thick-disk and halo dwarf stars in the present survey. The extensions to the brighter and fainter absolute magnitudes are the high-metallicity luminosity functions taken from Da Costa (1982) and Wielen et al. (1983), and scaled to the lower metallicities.

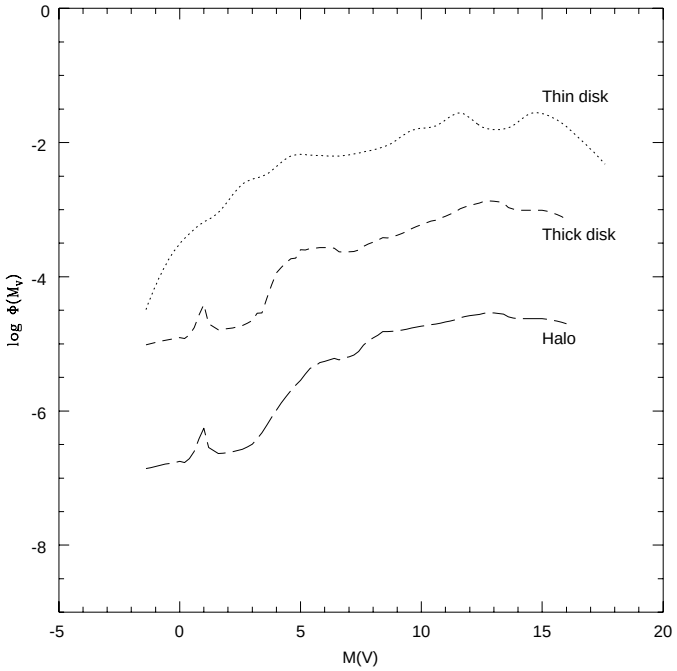

Fig. 10. Luminosity functions for the Galactic components investigated in the present analysis. The thin-disk LF provided by the HIPPARCOS data is assumed to represent solar metallicity ([M/H]=0.0) and has been taken from Jahreiss & Wielen (1997); the thick-disk and halo LFs have been interpolated from the original data of Fig. 9 to metallicities $[M/H] = (-0.625, -1.75)$ initially adopted for these components.

luminosity functions (LFs) adopted for the different population components and their subsequent transformation from the original Johnson-standard UBV to the actual survey-standard RGU systems. In this subsection, we discuss improvements over the preliminary results of Paper I that we should expect from new luminosity function and color transformation data.

2.3.1. Luminosity functions

It has been well known for quite some time that LF features, such as the so-called "globular cluster feature" (Bahcall et al. 1985), the "Wielen dip" (Bahcall & Soneira 1983), or the changes in LF shape implied by limited resolution of binary stars and multiple systems (Buser & Kaeser 1985), have important effects on predicted star count and color field-survey data in different ranges of apparent magnitude. Thus, the initial strategy followed in Paper I has been to use component-specific LFs which account for perhaps the crudest of real differences that we should expect to exist between the LFs pertaining to the different components.

Accordingly, all calculations have so far been performed assuming the component-specific LFs discussed in Paper I. Three properties of these functions should be recalled here: (1) the thin-disk LF has been based on the Gliese (1969) catalog of nearby stars and was derived by Buser & Kaeser (1985), anticipating that a sizeable fraction of the individual members of binary and multiple systems in the source catalog would remain unresolved if seen from the larger distances sampled in the present RGU data; (2) the thick-disk and halo LFs have been assumed to have the same shapes (though not the same local normalizations, of course), given by Da Costa's (1982) LF derived for the intermediately metal-poor ([M/H]=-0.85) globular cluster 47 Tuc, supplemented by Wielen et al.'s (1983) thin-disk LF for the fainter stars; (3) for each of these LFs, the local normalization has been left as a free parameter whose (optimized) value is to be determined from the actual analysis of the observed RGU data.

The results of our preliminary analysis of Paper I have now led us to subject these original precepts to revision, as follows.

1. HIPPARCOS data. The effect of low spatial resolution on the (apparent) local LF is less significant than anticipated, essentially because the relevant resolution limit is set by stars seen at distances > 1 kpc, which is true for a small fraction of thin-disk stars only in most fields of the new Basel high-latitude survey. Thus, for the resolution-corrected LF originally calculated from the Gliese (1969) catalog by Buser & Kaeser (1985), we now substitute the thin-disk LF derived by Jahreiss & Wielen (1997) from the superior HIPPARCOS data for the local stellar individuals. As can be seen in Figs. 10 and 11 below, this new LF is not quite as smooth as the original Buser & Kaeser LF but exhibits several rather strong features. Note however that the most pronounced of these, at $11 < M_V < 15$, is irrelevant to the present analysis, since such stars are much too faint to be sampled in any significant number in the new Basel survey.

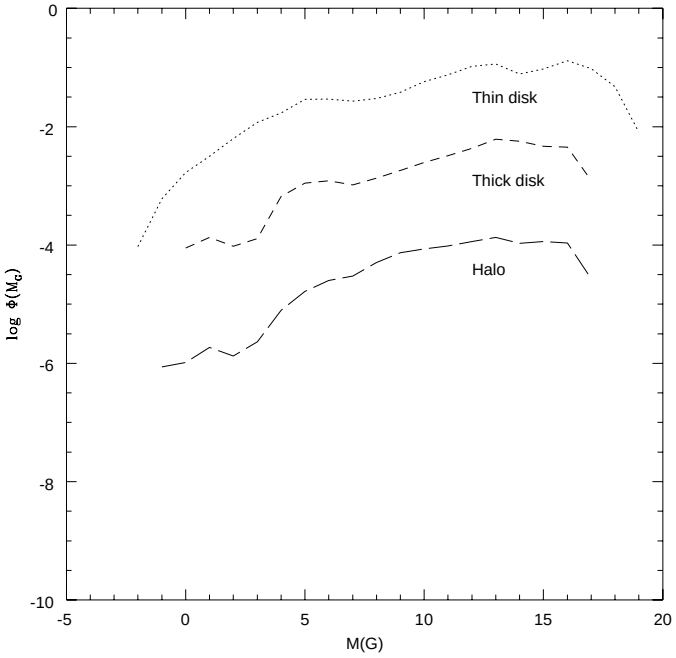

Fig. 11. Same as Fig. 10, but transformed from the Johnson-V to the Basel-G system of absolute magnitudes (see text).

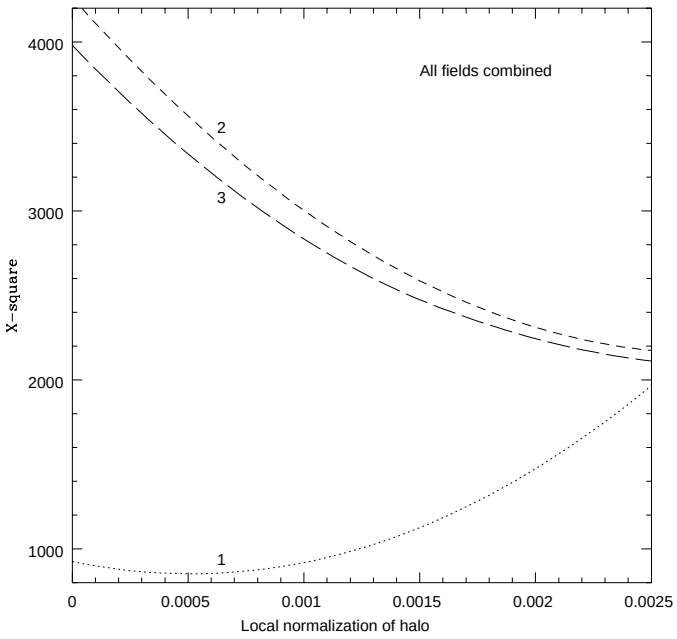

Fig. 12. χ^2-curves for models assuming thick-disk LF to be indistinguishable in shape and metallicity either from the thin-disk LF (2) or from the halo LF (3), compared to result obtained assuming a distinct LF for each component (1). Models (2) and (3) clearly compensate for the implied loss of discrimination by accomodating the metal-poor thick-disk stars preferentially in the halo, leading to an excess local density of halo stars. Note that the best of these latter models have higher χ^2_{min}-values by a factor of ~ 2 over the best models of curve (1)!

2. Metallicity dependence. McClure et al. (1986) were among the first to provide observational evidence for a possible dependence of the luminosity functions on stellar metallicity in Galactic globular clusters. Although, or even just because, the reality of such a metallicity dependence has been extremely difficult to establish and is, in fact, still a matter of debate, these cluster-LFs given by McClure et al. may at least provide a more appropriate representation of possible LF variations which are to be expected among the different observed field-star population components in the Galaxy. In particular, they can be used for a more continuous and consistent interpolation between the LFs of the local thin disk and the extreme halo than is possible from the approach employed thus far: while the 47 Tuc LF used in Paper I for the thick disk and the halo may just suffice to account for the major differences between two discrete populations separated by order of $\sim$ 1 dex or more in mean metallicities, it is almost certainly inadequate for matching at least three real populations that also have large and even mutually overlapping metallicity dispersions which altogether cover (essentially) the full observed metallicity range of more than 2 dex. If there should indeed be a metallicity dependence of the stellar LF of the kind suggested by the globular cluster study of McClure et al., the improved power to measure photometric metallicity effects by well-calibrated broad-band systems (such as the Basel RGU or the Washington CT_1T_2M systems) provides hope for answering the important question of whether this metallicity dependence is also present in the LFs of the field-star populations. If successful, the result will (more or less) directly translate into the corresponding (now suspected) metallicity dependence of the underlying IMF (McClure et al. 1986) and/or mass-luminosity relation (von Hippel et al. 1996), and will eventually allow us to provide a more physical interpretation of the present empirical structural models in terms of luminosity functions derived from theoretical calculations of the evolution of star formation and chemical enrichment of the large-scale Galactic field-star populations.

Thus, in the present paper, we expand the LF options in the following way: for the thick-disk and halo main sequence stars, i.e, with absolute magnitudes $4^m \leq M_V \leq 9^m$, we substitute the LFs given by McClure et al. (1986) for globular clusters of different metallicities, shown in normalized form in Fig. 9. These LFs are interpolated to the metallicities [M/H] = (-0.625, -1.75) initially adopted for the thick-disk and the halo components. Fig. 10 illustrates the resulting new set of LFs adopted in the present Paper for all three main components, while Fig. 11 gives these same LFs as transformed (from Fig. 10) to RGU, and as actually used in calculating the predicted star count and color distributions of the present survey.

2.3.2. Color-magnitude transformations for red stars

As anticipated in Paper I (Figs. 12-15) and evidenced here again in Fig. 2, almost all the model calculations still fail to reproduce reliably the red tails of the observed color distributions. One of the likely reasons is lying with the limited range of application of the photometric transformations used between the calibration standard-UBV and the survey standard-RGU systems.

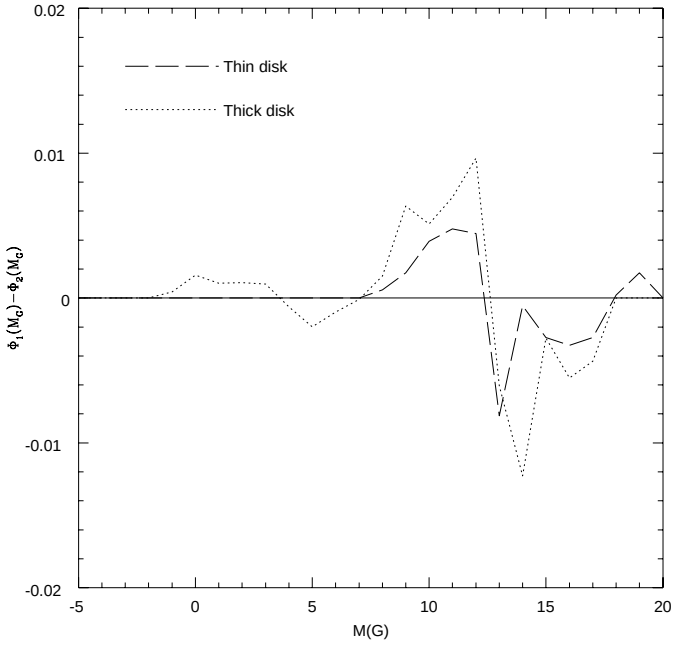

Fig. 13. Differences between LFs transformed to RGU from UBV [Fig. 10] with [Φ_2] or without [Φ_1] taking into account the separate equations applying to the red M-stars in Table 3. Thus, areas above the zero-line measure the number of stars which, upon including the red-star transformations, are subtracted from the corresponding absolute magnitude interval in the original LF used in Paper I [i.e., Φ_1], and which are shifted to fainter absolute magnitudes where the LF is accordingly increased [areas below the zero-line].

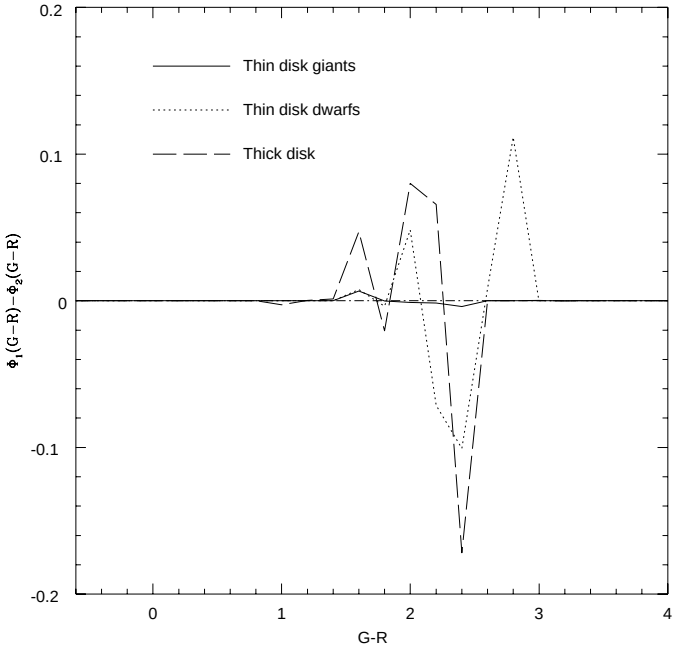

Fig. 14. Same as Fig. 13, but with LF differences now expressed as functions of G-R color. Note that the nonuniform shifts to redder colors for the different components (insert) may lead to either depletion, compensation, or amplification of resulting total star counts in different color intervals (Fig. 15), depending on the relative count contributions of the thin- and thick-disk components, such as those predicted in the model shown in Fig. 16.

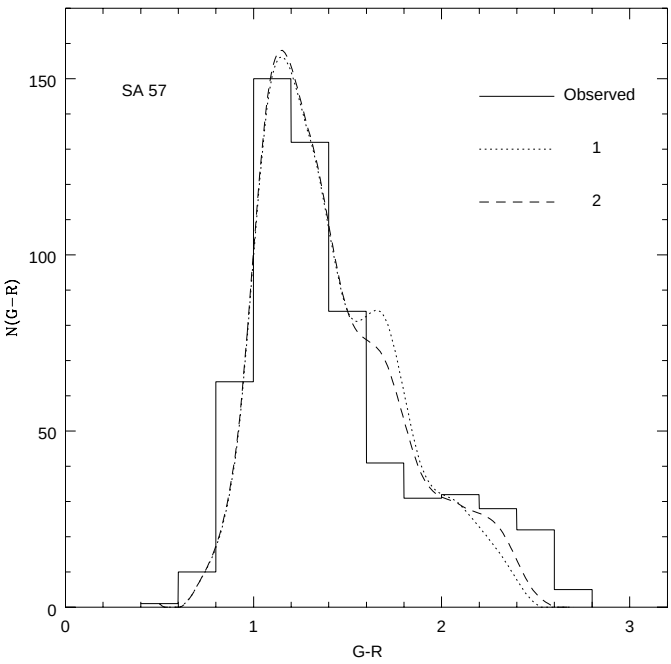

Fig. 15. Improved match of observed and predicted red wings of G-R color distribution in SA57. Both predicted curves have been computed for the same structural model of the Galaxy; the only difference between the two is that the dashed curve (2) includes the full transformation matrix of Table 3, while the dotted curve (1) does not include the M-star transformations. See the text.

In the exploratory calculations of Paper I, as the simplest approximation for converting the luminosity functions from extant UBV data to the RGU system, a single set of transformation equations were used for the full ranges of stellar types O through M. However, due to their strong atomic and molecular absorption features, the reddest dwarfs and giants, of spectral type M at $B-V>1.40$, do not share the same transformation properties with the bluer stars, which have smoother spectral flux distributions. In fact, O-K-star transformations will lead to derived RGU colors and magnitudes for M-stars with systematic errors of up to 0.4 magnitudes bluer and brighter than observed (Buser 1988). It is obvious, then, that the calculations should be substantially improved by introducing separate transformation equations for these coolest objects in the new Basel survey catalog.

Thus, in the present new model calculations we have implemented Table 3, which gives the full matrix of coefficients applying to the transformation equations

$$C = a\cdot(U-B)+b\cdot(B-V)+c,$$

where C is one of the color indices (G-V), (G-R), or (U-G). This matrix was derived by Buser (1988) from observed spectrophotometric flux distributions of normal Population I stars, and explicitly accounts for the spectral differences and their implied differences in transformation properties existing between O-K- and M-type stars and also between dwarfs and giants of either of these two varieties. For stars having colors in the interval $1.3\le B-V\le 1.4$, simple averages obtained from the

Table 3. Transformation coefficients for $C = a \cdot (U-B) + b \cdot (B-V) + c$

$C = (G-V)$		a	b	c	B-V color range	std. error of estimate
O-K	dwarfs	-0.01	0.63	-0.01	≤ 1.4	0.011
M	dwarfs	-0.46	0.88	0.24	≥ 1.3	0.039
A-K	giants	-0.02	0.65	-0.01	≤ 1.4	0.012
M	giants	-0.52	1.36	-0.12	≥ 1.3	0.022
$C = (G-R)$		a	b	c	B-V color range	std. error of estimate
O-K	dwarfs	-0.04	1.27	0.32	≤ 1.4	0.022
M	dwarfs	-0.99	1.13	1.76	≥ 1.3	0.039
A-K	giants	-0.09	1.22	0.33	≤ 1.4	0.021
M	giants	-0.93	2.36	0.31	≥ 1.3	0.060
$C = (U-G)$		a	b	c	B-V color range	std. error of estimate
O-K	dwarfs	1.17	0.15	1.24	≤ 1.4	0.013
M	dwarfs	1.21	0.23	1.05	≥ 1.3	0.024
A-K	giants	1.12	0.15	1.24	≤ 1.4	0.008
M	giants	1.36	-0.29	1.47	≥ 1.3	0.018

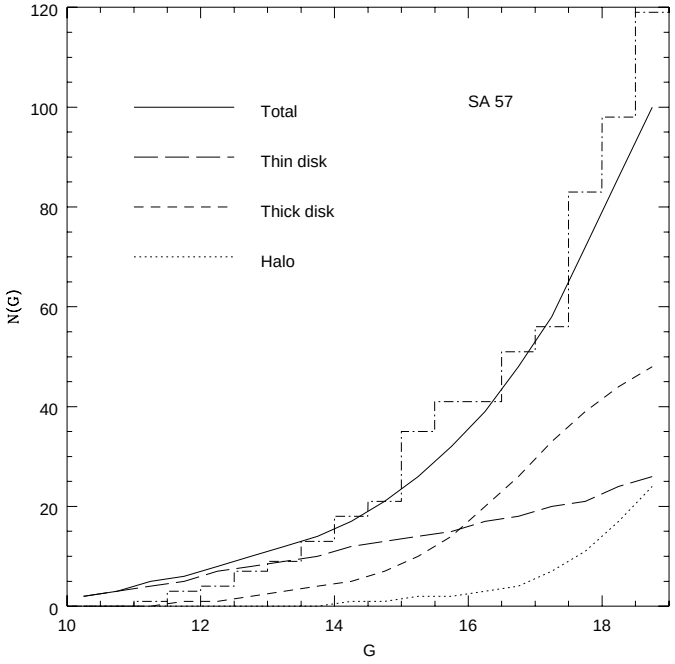

Fig. 16. Star counts N(G) in the SA57 field, comparing the observed histogram with the predicted total built up by the contributions from the individual components. The thin disk dominates down to $G = 16$ but is overtaken by the thick disk and the halo at fainter magnitudes.

relevant "blue" and "red" equations provide a smooth transition between the different transformations.

In general, these equations allow us to derive transformed colors and magnitudes with a systematic accuracy on the level of a few hundredths of magnitude. Note that the above equations have been used in calculating the one- and two-dimensional star count distributions $N(G)$, $N(G-R)$, and $N(G, G-R)$ for all the stellar population components, irrespective of their different metallicities adopted in the model. Although not strictly correct, this approximation can be (temporarily) justified by the fact (Buser 1988, Güngör Ak 1995) that metallicity should be expected to have a significant effect on the transformations to the ultraviolet color index U-G only, but to be of considerably lower importance for G and G-R. However, for a fully consistent analysis, a complete set of transformation equations as functions of stellar metallicity [M/H] is being worked out (Buser et al. 1998b) from synthetic photometry of a new comprehensive library of theoretical stellar spectra (Lejeune et al. 1997, 1998), and will be applied to the all-survey RGU data in later papers of this series.

3. New model calculations and results

As in our previous studies (e.g., Fig. 5 of Paper I), the two-dimensional $N(G, G-R)$ data were found to be fairly insensitive to the local density parameter of the thin disk, n_0. In fact, models computed based on the HIPPARCOS LF with n_0 in the range 0.07-0.12 stars$/pc^3$ provide χ^2-fits to our data which are only marginally different, and thus a value $n_0 = 0.11$ stars$/pc^3$ was adopted for all subsequent model calculations, in agreement with the value derived from the HIPPARCOS data for the very local sphere by Jahreiss & Wielen (1997).

Based on the improved input discussed in the preceding section, 28,800 new models have then been computed as follows: optimized mean values for the (remaining) five secondary model parameters were taken from Table 3 in Paper I, while the six primary parameters (to be discussed below), including three for the thick-disk component, were allowed to vary within their adopted original or new extended ranges given in Tables 2 of Paper I and the present paper, respectively. From these new models, star count and color distributions were finally calculated and compared to the observed data for each of the seven fields plus their combined survey.

In order to assess the extent of the improvement and to derive optimized parameter values, we here employ again the analysis tools and procedures developed in Paper I, where $\chi^2_{1,k}, k \in [1,7]$ and $\chi^2_{1,s} = \sum_{k=1}^{7} \chi^2_{1,k}/7$ are used as the basic estimators of goodness of fit of the model predictions to the data for each of the seven individual fields and for the combined survey in all seven fields, respectively. In particular, the individually or glob-

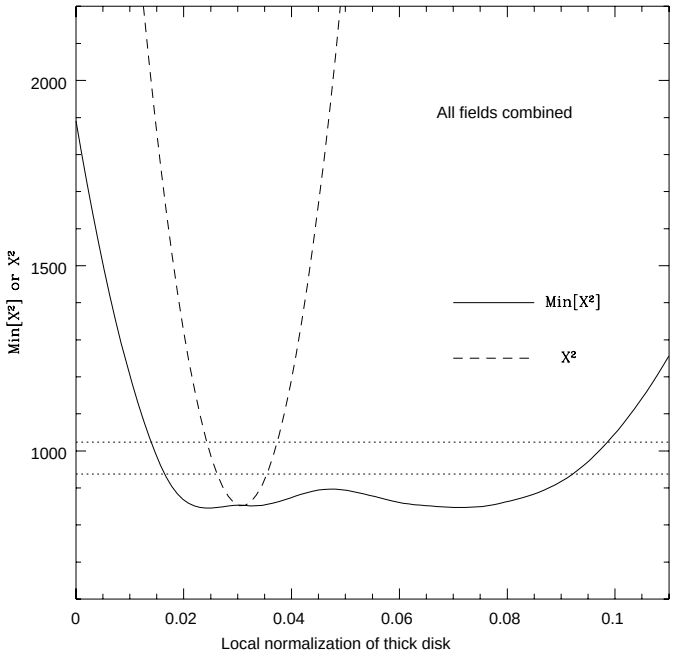

Fig. 17. $Min[\chi^2(p_i)]$-curve for $p_i = n_1$, the local density of the thick disk, derived from the combined survey of seven fields and for the *new* parameter range adopted in this paper. Horizontal lines indicate selection limits of good models having $\chi^2_{max}(n_1) \leq \xi \times \chi^2_{1,s,min}$, where $\xi = 1.1$, i.e., $\chi^2_{max}(n_1) = 938$, and $\xi = 1.2$, i.e., $\chi^2_{max}(n_1) = 1024$, respectively. To illustrate the difference with the $Min[\chi^2]$-curve, the χ^2-curve for the the global minimum has also been plotted. Compare with Fig. 3.

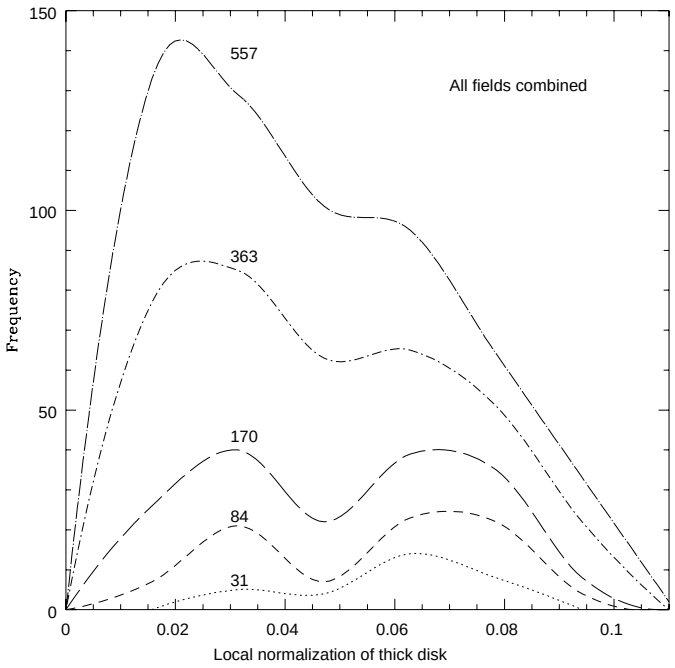

Fig. 18. Frequency distributions $F(p_i, \xi)$ for $p_i = n_1$, the local density of the thick disk, derived from the combined survey of seven fields and for the *new* parameter range adopted in this paper. The sequence of curves from bottom to top corresponds to values of ξ growing from 1.1 to 1.5; labels indicate the number of models involved. Compare with Fig. 4.

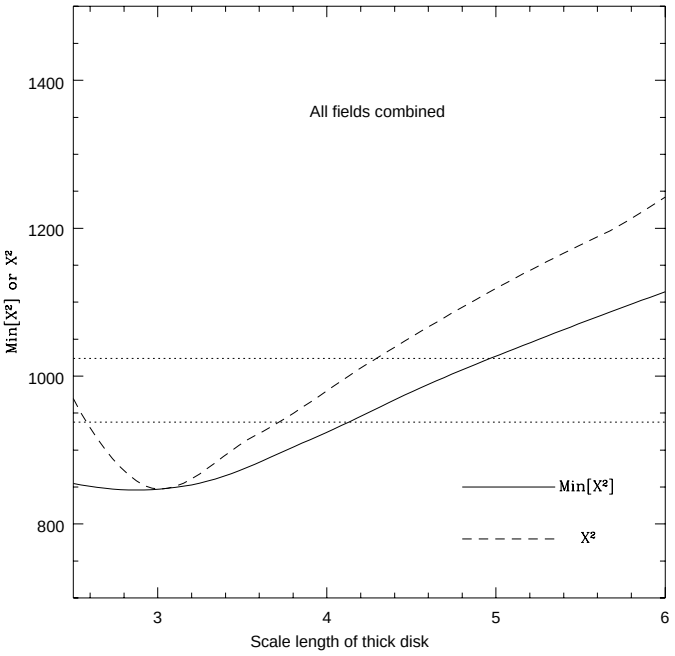

Fig. 19. $Min[\chi^2(p_i)]$-curve for $p_i = d_3$, the scale length of the thick disk, derived from the combined survey of seven fields and for the *new* parameter range adopted in this paper. Horizontal lines indicate selection limits of good models having $\chi^2_{max}(d_3) \leq \xi \times \chi^2_{1,s,min}$, where $\xi = 1.1$, i.e., $\chi^2_{max}(d_3) = 938$ and $\xi = 1.2$, i.e., $\chi^2_{max}(3_3) = 1024$, respectively. To illustrate the difference with the $Min[\chi^2]$-curve, the χ^2-curve for the the global minimum has also been plotted. Compare with Fig. 5.

ally best-fitting models are identified by $\chi^2_{1,k,min}$ and $\chi^2_{1,s,min}$, respectively, and serve as pivots for the subsequent selection of models used in calculating optimized parameter values.

3.1. General improvements

The main general result is that $\chi^2_{1,s,min}$ has dropped now to 853, which is almost 25% below the corresponding value obtained for the globally best model in Paper I. (Incidentally, this means that the globally best model of Paper I now does not even make it into the $\xi = 1.2$-selection of good models from which the optimized parameters will be determined below!) While this result stems from the combination of the different improvements to the model input described above, the individual contributions can be roughly traced as follows.

Perhaps the most important effect is traceable to the new luminosity functions (LFs). All the lowest-χ^2 models include the LFs shown in Figs. 9-11, which have distinctly different shapes on account of their (adopted) underlying metallicity differences. Calculations for a thick-disk LF whose shape and metallicity are indistinguishable from either the thin-disk or the halo LF invariably result in χ^2_{min} scores which exceed those obtained from the three distinct LFs in Fig. 11 by factors larger than 1.5, up to 2.5. This appears most prominently in its effect upon the halo normalization, n_2, and is illustrated in the χ^2-curves of Fig. 12: while the χ^2 for all the models involving two different LFs only [i.e., curves (2) and (3)] are in no way competitive with the

lowest-χ^2 obtained for the models based on three different LFs [i.e., curve (1)], even the best 2LF-models, at the right edge of Fig. 12, tend to accommodate too many stars with the halo, leading to too large a local normalization for that component. In fact, this LF-effect is very similar to the effect produced by the weakening or even annihilation of the thick disk demonstrated in Table 1 and discussed in Sect. 2.1.

We thus conclude that the data of the new Basel survey provide strong evidence for each of the three main Galactic population components[1] having its own (local) LF characterized by a distinctly specific shape and metallicity.

The more detailed transformation equations of Table 3 have basically two effects on the model predictions, since they imply changes of both the absolute magnitudes and the colors of the stars. First, as shown in Fig. 13, the M-star transformations predict fainter absolute G magnitudes than are obtained from the O-K-star transformations, leading to redistribution of apparent magnitudes and, consequently, also of the star counts, $N(G)$. If applied to a (rising) LF – as, e.g., in the interval $\sim 7 \leq M_V \leq\sim 9$ in Fig. 10 – this may eventually also lead to a decrease in predicted numbers of red main sequence stars, because a larger fraction of these may then be pushed beyond the observed apparent magnitude limit of the survey data than are replenished from the brighter magnitude bins.

Second, the M-star transformations also predict redder colors than would be obtained from the O-K-star transformations. Fig. 14 illustrates this effect on the luminosity function, and Fig. 15 gives a typical example (SA 57) of how the effect eventually propagates into the field-star G-R color distribution, whose final shape depends on the relative model-predicted star counts contributed by the individual components, as shown in Fig. 16.

Note that the two predicted color curves in Fig. 15 result from calculations which are identical except for the two different transformation models employed in converting the LFs of Fig. 10 from UBV to the RGU system. The more adequate transformations lead to: (1) significant redistribution of the stars from colors $1.5 < G-R < 2$ to the redder interval $G-R > 2$, (2) a closer match of the predicted color distribution with the observed histogram, and (3) a reduction of χ^2_1 by $\sim 18\%$, as calculated from the fits to the combined two-dimensional $N(G, G-R)$ data.

Since in this field the reddest stars predominantly belong to the thick-disk component – which is shown in Fig. 16 to dominate the stellar census at $m_G \geq 16$ –, we expect to improve the fit still further in a later paper of this series, when even more appropriate transformations will be available for these lower-abundance stars.

3.2. Optimized parameter values and constraints

Based on the total of 28,800 new models, the improved model fits to the star count and color data described above are now used to analyse their impact on the six primary structural parameters, $p_i, i \in [1,6]$ (cf. Table 4). For each of these parameters, results for the combined survey of seven fields are given in terms of the $Min[\chi^2(p_i)]$-curve and its associated frequency distributions, $F(p_i, \xi)$, as follows. For each specific value adopted by a particular parameter, its actual minimum value of $\chi^2_{1,s}$, $Min[\chi^2(p_i)]$, is calculated from *all* the new models, whose 5 remaining free primary parameters (cf. Table 4) are allowed to vary throughout their original adopted or new extended ranges. Thus, the $Min[\chi^2(p_i)]$-curves trace out the best-fitting model existing at each value of the particular parameter, p_i.

Obviously, the globally best model defined above is then identified by $\chi^2_{1,s,min} = Min\{Min[\chi^2(p_i), i \in [1,6]]\}$. Subsequently, models are selected according to the condition $\chi^2(p_i) \leq \chi^2_{max}(p_i) = \xi \times \chi^2_{1,s,min}$, where $\xi \in [1.1, 1.5]$, and the frequency distributions of parameter values, $F(p_i, \xi)$, are evaluated as functions of ξ. Hence, optimized parameter values, $\bar{p}_i$, and constraints, $\sigma_{\bar{p}_i}$, are finally determined from the good models ($\xi \leq 1.1$ and $\xi \leq 1.2$), using the parameter weighting scheme described in Paper I. Models satisfying this selection were shown in Paper I to be statistically consistent with the estimated external accuracy of the data on the two-sigma level.

3.2.1. Thin-disk and halo parameters

Before discussing the thick-disk parameters, we first check on the impact of the new LF input and photometric calibration (Sect. 2.3) on the thin-disk and halo primary parameters. The new results are reported in the third to fifth columns of Table 4, where the two bottom lines also give the corresponding preliminary results obtained in Paper I for the combined survey in seven fields.

Table 4 shows that the primary parameters of the thin disk, i.e., the optimized values $\bar{h}_1$ and $\bar{h}_3$ for the scale heights of the old and young dwarfs, respectively, are found to be lower than, but still within one sigma of their corresponding values derived in Paper I. While the mean scale height of the old thin-disk dwarfs, $\bar{h}_1 = (0.88 \pm 0.15) \cdot 325pc \simeq 290 \pm 50pc$, thus remains essentially unchanged, the somewhat larger dispersion seems to indicate that real deviations from the adopted smooth density model may exist in the data in the different field directions. This conclusion will be supported below by similar results obtained for two parameters of the thick-disk.

No significant changes have been found for the local density n_2 of the halo either. The new models provide an optimized mean value and (formal) constraints for this parameter which are almost the same as derived in Paper I. Thus, the main conclusion of this subsection is that the optimized parameter values of the thin-disk and halo components of our model are essentially robust against the changes in model input and photometric calibration implemented in the present investigation.

3.2.2. Thick-disk parameters

The optimized values and constraints derived for the thick-disk parameters are also summarized in Table 4 for both the individ-

[1] More precisely, we should speak of four components, since the young thin disk has its "own" LF as well – for the main sequence stars included in the bright tail of the HIPPARCOS LF.

Table 4. Optimized parameter values $\bar{p}$ of Galactic model

Field		Thin-disk and Halo			**Thick-disk**		
No.	Name	h_1	h_3	n_2	n_1	d_3	h_4
1	Praesepe	1.15	0.15	0.0016	**0.101**	**4.36**	**0.62**
2	M101	0.81	0.18	0.00002	**0.078**	**4.05**	**0.86**
3	M67	0.94	0.15	0.0014	**0.098**	**4.09**	**0.52**
4	SA54	0.81	0.15	0.0013	**0.026**	**4.14**	**1.11**
5	SA57	0.82	0.17	0.0014	**0.051**	**4.30**	**0.88**
6	SA141	0.98	0.14	0.0025	**0.038**	**4.26**	**0.60**
7	M5	0.90	0.12	0.0002	**0.073**	**4.10**	**0.94**
1-7	$\bar{p}_{1-7}$	0.88	0.14	0.00045	**0.059**	**3.00**	**0.91**
	$\sigma_{\bar{p}_{1-7}}$	0.15	0.03	0.0003	**0.03**	**1.5**	**0.30**
Paper I	$\bar{p}_{1-7}$	0.90	0.17	0.0005	0.054	4.25	1.15
	$\sigma_{\bar{p}_{1-7}}$	0.1	0.03	0.0003	0.015	1.0	0.15

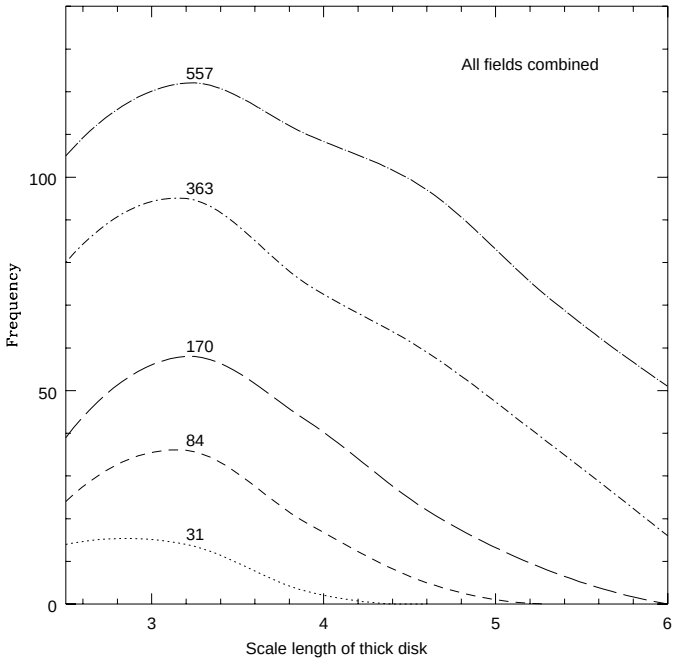

Fig. 20. Frequency distributions $F(p_i, \xi)$ for $p_i = d_3$, the scale length of the thick disk, derived from the combined survey of seven fields and for the *new* parameter range adopted in this paper. The sequence of curves from bottom to top corresponds to values of ξ growing from 1.1 to 1.5; labels indicate the number of models involved. Compare with Fig. 6.

ual fields and the combined survey of seven fields. Two principal steps toward these results are illustrated in Figs. 17-22 for each of these parameters, which we shall now briefly discuss.

The local density parameter n_1 is explored in Figs. 17 and 18, which should be compared with its χ^2-curve and frequency distributions previously derived in Paper I and given in Figs. 3 and 4. The most significant new result is that the best models have almost uniform $Min[\chi^2(n_1)]$ for parameter values $0.02 \leq n_1 \leq 0.09$, and good models can thus be found throughout this same range, which is significantly more extended than in the preliminary analysis reported in Figs. 3 and 4. [2] Still, the maximum at $n_1 \sim 0.06$ of the (new) frequency distribution for the best models ($\xi = 1.1$) in Fig. 18 corroborates the original result derived in Paper I for the optimized mean value of the thick-disk local density, $\bar{n}_1 = 0.054 n_0$, while the flatter secondary peak near $n_1 \sim 0.03$, which becomes fully pronounced in the frequency distribution for the $\xi = 1.2$ models, however demonstrates that the earlier constraint on this parameter, $\sigma_{\bar{n}_1} = 0.015$ (Paper I), was too strong. In fact, Table 4 shows that this constraint is now relaxed to $\sigma_{\bar{n}_1} = 0.03$, which is a measure of the dispersions exhibited by the optimized parameter values of the individual fields, and which, therefore, reflects considerable large-scale deviations from the adopted smoothness of the global thick-disk density distribution.

Similar results for the scale length parameter d_3 are presented in Figs. 19 and 20. As in Figs. 5 and 6 above, the relatively small amplitudes of the χ^2- and $Min[\chi^2]$-curves confirm the low sensitivity of the present data to this parameter, anticipated in the preliminary analysis. This low sensitivity is also evidenced by the very flat frequency distributions obtained for the individual fields, whose weak local maxima at or near ~ 3 kpc however accumulate to the somewhat more pronouncedly peaked frequency distribution shown in Fig. 20 and the correspondingly low optimized value for the combined survey given in Tab 4. In this case, the larger dispersion primarily measures the uncertainty in derived parameter values $\bar{d}_3$.

[2] Note the important difference with the χ^2-curve, which illustrates how the *goodness of fit* to the data (measured by χ^2) changes about its optimum (i.e., where $\chi^2 = Min$) if a particular parameter changes (e.g., in Fig. 3: n_1, the local normalization of the thick disk) while all other parameters are kept fixed (in the present calculations: at their optimized values derived here or in Paper I). In contrast, the $Min[\chi^2]$-curve describes the change of the *optimum fit* to the data (measured by $Min[\chi^2]$) achievable at any adopted value of a particular parameter (e.g., in Fig. 17: n_1, the local normalization of the thick disk) and upon variation of all other parameters within their permissible ranges (in the present calculations: 2 for the thin disk, 2 for the thick disk, and 1 for the halo).

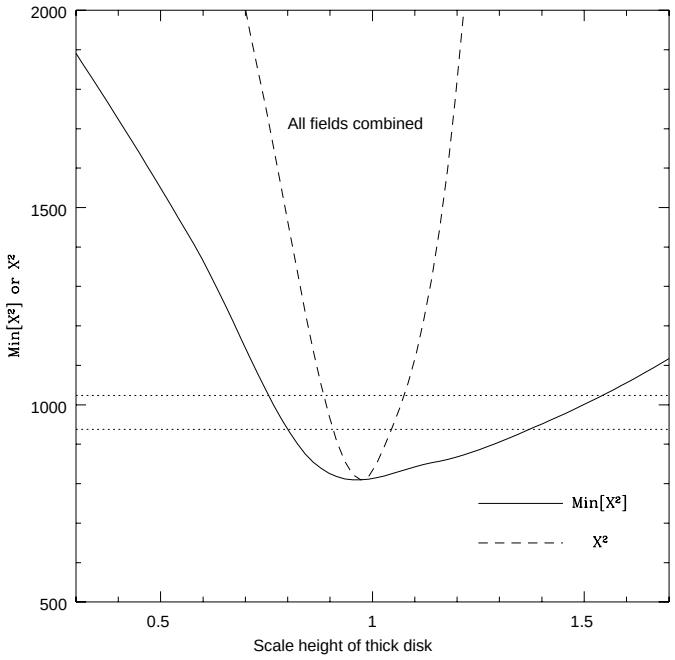

Fig. 21. $Min[\chi^2(p_i)]$-curve for $p_i = h_4$, the scale height of the thick disk, derived from the combined survey of seven fields and for the *new* parameter range adopted in this paper. Horizontal lines indicate selection limits of good models having $\chi^2_{max}(h_4) \leq \xi \times \chi^2_{1,s,min}$, where $\xi = 1.1$, i.e., $\chi^2_{max}(h_4) = 938$ and $\xi = 1.2$, i.e., $\chi^2_{max}(h_4) = 1024$, respectively. To illustrate the difference with the $Min[\chi^2]$-curve, the χ^2-curve for the the global minimum has also been plotted.

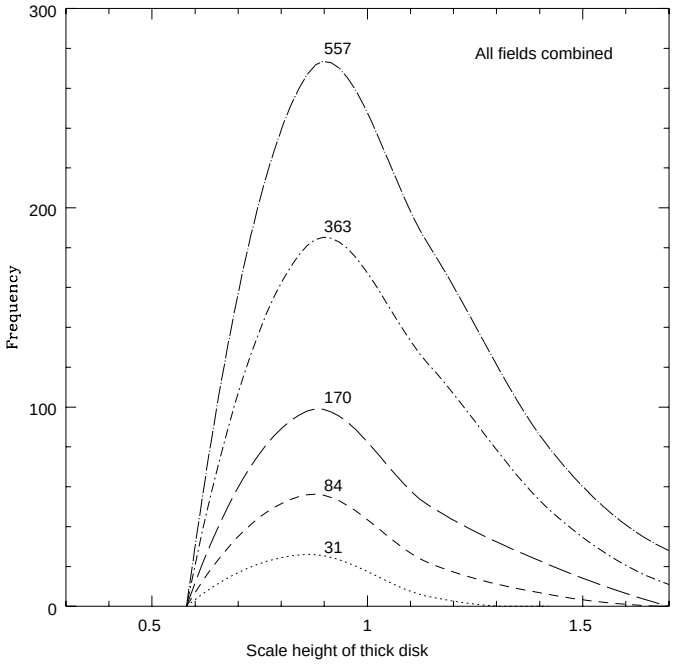

Fig. 22. Frequency distributions $F(p_i, \xi)$ for $p_i = h_4$, the scale height of the thick disk, derived from the combined survey of seven fields and for the *new* parameter range adopted in this paper. The sequence of curves from bottom to top corresponds to values of ξ growing from 1.1 to 1.5; labels indicate the number of models involved. Compare with Figs. 7 and 8.

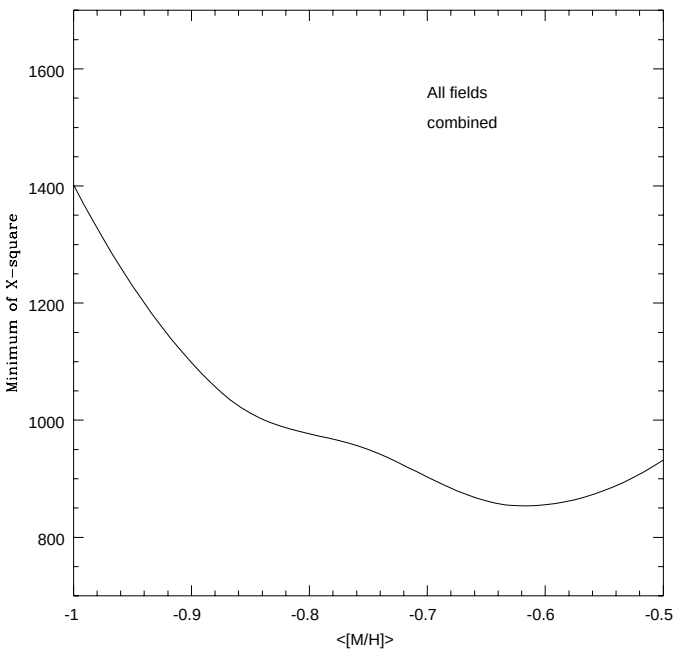

Fig. 23. $Min[\chi^2]$-curve for $\langle[M/H]\rangle$, the mean metallicity of the thick disk, derived from the combined survey of seven fields and from the improved structural models calculated in this paper. See the text.

On the other hand, the χ^2- and $Min[\chi^2]$-curves and the frequency distributions displayed in Figs. 21 and 22 again demonstrate convincingly that the present data provide excellent sensitivity to the scale height parameter, h_4. The sharp minimum of $Min[\chi^2]$ and peaks of $F(h_4, \xi)$ indicate that an optimized mean value and constraints of this parameter can now be derived unambiguously from the combined data in all seven fields analysed here. Indeed, as shown in Table 4, they result in a lower mean value but also a larger dispersion than was found for the thick-disk scale height in the preliminary analysis of Paper I. In fact, the larger dispersion is in part a natural consequence of the density law, where the intrinsic (anti-)correlation between the local normalization and the scale height provides one of the gauges for matching the models and the data *in an individual field*. Because an optimized parameter value for the *combined survey* is calculated from the best models satisfying a *field-independent* constraint, models for individual fields having parameter values near their (individual) optimum values have usually higher chances of entering the above full-survey selection. Accordingly, the wider range in n_1 found for the good models in Figs. 17 and 18 then also goes along with the broader dispersion in h_4 revealed in Figs. 21 and 22.

3.3. Thick-disk metallicity structure

Although this "ultimate" goal of the present project will be attempted definitively only in a later paper – based on the complete survey data in all 14 fields and the full synthetic calibration of the metallicity-sensitive U-G colors –, for completeness we add a few comments on results obtained beyond Paper I, derived now from the new improved structural model calculations described

above. Mean metallicities and metallicity gradients of the thick disk have been determined following the procedure detailed in Paper I, except that both vertical *and* radial gradients have now been included. Thus, the metallicity of the thick disk component is modelled as

$$[M/H] = a + b \cdot |z| + c \cdot (x - r_0),$$

where $b = \partial[M/H]/\partial z$, $c = \partial[M/H]/\partial x$ are the vertical and radial metallicity gradients, respectively; x and z are the galactocentric cylindrical coordinates of a given point (distance from the Galactic center projected upon the Galactic plane, and height above the Galactic plane, respectively), and r_0 is the distance of the sun from the Galactic center (assumed to be 8.6 kpc).

The main result is that the differences with the preliminary results of Paper I are insignificant. In fact, the radial gradients are found to be $|c| < 0.04$ dex/kpc in all seven fields, and the vertical gradient, $\langle b \rangle = \langle \partial[M/H]/\partial z \rangle = -0.10 \pm 0.10$ dex/kpc, and mean metallicity, $\langle [M/H] \rangle = -0.63 \pm 0.15$ dex, derived for the combined survey, come out almost the same as in Paper I. The $Min[\chi^2]$-curve in Fig. 23 shows that the above optimized value for the mean thick-disk metallicity, $\langle [M/H] \rangle$, is well determined from the best models for the combined survey of seven fields, with a standard error of estimate of only ~ 0.15 dex; however note (again) that the actual dispersion $\sigma_{\langle [M/H] \rangle}$ may be (significantly) larger,[3] as this quantity is obtained from the distribution of $\langle [M/H] \rangle$ pertaining to the individual fields. In fact, $\sigma_{\langle [M/H] \rangle} \sim 0.4$ dex, which is again indistinguishable from the result of Paper I.

Thus, while the present analysis essentially confirms our earlier results, the available data still – but not unexpectedly – do not provide conclusive evidence of any systematic finer structure, such as a radial and/or a vertical gradient, of the thick disk's larger-scale metallicity distribution.

4. Discussion and conclusions

Since the important paper of Reid & Majewski (1993) on the analysis of deep star counts in the North Galactic Pole (NGP) field SA 57, a number of publications have appeared which are based on new analyses of the same and/or similar data from new Galactic survey work. Apart from the unidirectional survey of the NGP by Spagna et al. (1996), Robin et al. (1996) and Ng et al. (1997) also investigate several fields at intermediate latitudes along the Galactic meridian, including SA 54 and M5 (which are also part of the present survey). The first two of these recent studies make use of broad-band multicolor photometric *and* proper motion data, and all three of them provide analyses of the data in terms of appropriately consistent combinations of models including the kinematics, space density distributions, histories of star formation, and chemical evolution of the Galactic stellar populations.

Obviously, the combined aggregate of these survey data has large statistical weight which, along with the different methodologies chosen for the different analyses, should provide a substantial standard for assessing the reliability of the thick-disk picture that can currently be derived from such approaches. We shall thus present a brief comparison with the present work.

Determinations of relevant Galactic thick-disk properties are summarized in Table 5., where ρ/ρ_0 is the local density normalization in percent of the local thin-disk density, d and h are the exponential scale length and scale height, respectively, and $\langle [M/H] \rangle$ is the mean metallicity. Generally speaking, the overall average parameter values resulting from the recent individual studies are still well described by the plain figures given in the review by Morrison (1996). In particular, the results of the present paper are in excellent agreement with this global picture of the thick disk – which is all the more remarkable as they were derived from photometric data only, i.e., without supplementary information from proper motions!

The important next question then concerns the reliability of this global thick-disk model: how well do we now know the constraints to its parameters? Obviously in Table 5, there is (still) substantial dispersion among the different determinations of the scale height. In fact, the tabular data are (weakly) anti-correlated with the local density parameter in the sense that higher densities are associated with lower scale heights, or, for that matter, with lower Galactic latitudes. As anticipated in Sect. 3.2.2 above, this should however be expected if the star counts observed in a given field are fitted by a density model of the form $D \sim \rho \exp(-z/h)$, and is indeed also conspicuous in the resulting best-fitting data given for the seven individual fields of the present multi-directional survey in columns 6 (n_1) and 8 (h_4) of Table 4. On the other hand, as exposed in detail in Paper I and again in Sect. 3 above, calculation of the optimized parameter values for the combined survey explicitly accounts for this model dependency by including all model solutions that satisfy the constraint set by the (external) accuracy of the data for all seven fields simultaneously. Thus, the optimized mean parameter values are associated with relatively large dispersions, which however also appear to adequately accommodate the dispersions exhibited by the independent studies of Table 5.

In summary, the present data and analysis corroborate the larger-scale structural picture of the thick disk which has gradually emerged over the past years. We have demonstrated that, even though it is possible to describe this component by an average model specified by a unique set of parameter values, the actual constraints on these values, as derived from either the present data or from the current literature, do not appear to be very narrow. We cannot yet discard as insignificant the sizeable dispersions in local densities and, particularly, in scale heights and also in mean metallicities. If, indeed, their significance can be established by an appropriate χ^2- test – which will be provided in Paper V based on the analysis of yet more comprehensive RGU data –, these larger dispersions may have to be taken as indications of nonuniformity in the physical and chemical makeup of the real thick disk – implying a likely nonmonotonic formation history of this component as well.

While such a conclusion would also be supported by the fact that we have found the thick disk to have a luminosity function

[3] For illustration, see again the analyses of the other thick-disk parameters in Figs. 17-22.

Table 5. Recent determinations of Galactic thick-disk properties

Reference	Method	$\rho/\rho_0[\%]$	d [kpc]	h [pc]	$\langle[M/H]\rangle$ [dex]
Reid & Majewski (1993)[1]	Review	2 - 11	(3.5)	700 - 2000	(-0.6)
Morrison (1996)	Review	5	3.5	1000	-0.5
Norris (1996)	Review	5		1000-1300	-0.6
Gilmore et al. (1995)	individual F-G stars				-0.7
Robin et al. (1996)[2]	UBV star counts & p.m.	5.6 ± 1	2.8 ± 0.8	760 ± 50	-0.7 ± 0.2
Spagna et al. (1996)[3]	BVR star counts & p.m.	4.3		1137 ± 61	
Ng et al. (1997)	BV star counts	5.3	4.5	1000 ± 100	-0.75 - -1.5
Buser et al. (1998a)	RGU star counts	5.4 ± 1.5	4.25 ± 1.0	1150 ± 150	-0.6 ± 0.4
This paper	RGU star counts	5.9 ± 3	3.0 ± 1.5	910 ± 300	-0.6 ± 0.4

[1] Based on their Table 1B.
[2] Same model also shown consistent with star count and proper motion data discussed in Soubiran (1993), Ojha et al. (1994a,b), Perrin et al. (1995), and Haywood et al. (1997a,b).
[3] Study of North Galactic Pole (NGP) field exclusively.

which is distinctly different from those of the thin disk and halo, more definitive results on these issues can now be expected from the following next steps of this project.

1. Analysis of the second catalog of new homogeneous RGU survey data in seven additional intermediate-latitude ($20^\circ < |b| < 66^\circ$) fields will provide a more complete mapping and will allow us to obtain a more precise view of the "graininess" of the thick disk. In particular, two fields toward the center and anticenter directions should significantly enhance the reliability of the scale length determination, while from the distribution of the remaining fields we expect to gain a handle for breaking the "density-scale-height-degeneracy".
2. Implementation of a complete synthetic photometry-based calibration and transformation model for the UBV and RGU systems will provide the capability for full exploitation of the metallicity sensitivity of the RGU data (i.e., primarily of the U-G color) essentially down to the limit of photographic noise. From the combined survey of homogeneous, three-dimensional $N(G, G-R, U-G)$ data in 14 fields, we then expect to detect the presence or confirm the absence of large-scale metallicity gradients reliably enough for a significant discrimination of formation scenarios.

Acknowledgements. This work was supported by the Swiss National Science Foundation. J. Rong also acknowledges partial financial support by the Chinese National Natural Science Foundation (19733001).

References

Bahcall J.N., Soneira R.M., 1983, In: Philip A.G.D., Upgren A.R. (eds.) The Nearby Stars and the Stellar Luminosity Function. IAU Coll. 76, L. Davis Press, Schenectady, p. 209
Bahcall J.N., Ratnatunga K., Buser R., Fenkart R.P., Spaenhauer A., 1985, ApJ 299, 616
Buser R., 1988, In: Fresneau A., Hamm M. (eds.) Impacts des surveys du visible sur notre connaissance de la Galaxie. Comptes Rendus sur les Journées de Strasbourg, 9ème Réunion, Obs. de Strasbourg, p. 15
Buser R., Fenkart R.P., 1990, A&A 239, 243
Buser R., Kaeser U., 1985, A&A 145, 1
Buser R., Rong J.X., 1995, Baltic Astron. 4, 1
Buser R., Rong J.X., 1996a, In: Blitz L., Teuben P. (eds.) Unsolved Problems of the Milky Way. IAU Symp. 169, Kluwer, Dordrecht, p. 707
Buser R., Rong J.X., 1996b, In: Blitz L., Teuben P. (eds.) Unsolved Problems of the Milky Way. IAU Symp. 169, Kluwer, Dordrecht, p. 427
Buser R., Rong J.X., Karaali S., 1998a, A&A 331, 934 (Paper I)
Buser R., Westera P., Lejeune Th., Güngör Ak S., Rong J.X., 1998b, A&AS, in preparation
Casertano S., Ratnatunga K., Bahcall J.N., 1990, ApJ 357, 435
Costa G.S. da, 1982, AJ 87, 990
Gilmore G., Wyse R.F.G., Jones J.B., 1995, AJ 109, 1095
Gliese W., 1969, Veröff. Astron. Recheninst. Heidelberg No. 22
Güngör Ak S., 1995, Ph.D. Thesis, Istanbul Univ.
Haywood M., Robin A.C., Crézé M., 1997a, A&A 320, 428
Haywood M., Robin A.C., Crézé M., 1997b, A&A 320, 440
Hippel T. von, Gilmore G., Tanvir N., Robinson D., Jones D.H.P., 1996, AJ 112, 192
Jahreiss H., Wielen R., 1997, Proc. ESA Symp. Hipparcos Venice '97, ESA SP-402, Noordwijk, 675
Lejeune Th., Cuisinier F., Buser R., 1997, A&AS 125, 229
Lejeune Th., Cuisinier F., Buser R., 1998, A&AS 130, 65
McClure R.D., VandenBerg D.A., Smith G.H., et al., 1986, ApJ 307, L49
Morrison H.L., 1996, In: Morrison H., Sarajedini A. (eds.) Formation of the Galactic Halo...Inside and Out. ASP Conf. Ser. Vol. 92, p. 453
Ng Y.K., Bertelli G., Chiosi C., Bressan A., 1997, A&A 324, 65
Norris J., 1996, In: Morrison H., Sarajedini A. (eds.) Formation of the Galactic Halo...Inside and Out. ASP Conf. Ser. Vol. 92, p. 14
Ojha D.K., Bienaymé O., Robin A.C., Mohan V., 1994a, A&A 284, 771
Ojha D.K., Bienaymé O., Robin A.C., Mohan V., 1994b, A&A 290, 810
Perrin M.-N., Friel E.D., Bienaymé O., et al., 1995, A&A 298, 107
Reid N., Majewski S.R., 1993, ApJ 409, 635
Robin A.C., Haywood M., Crézé M., Ojha D.K., Bienaymé O., 1996, A&A 305, 125
Rose J.A., 1985, AJ 90, 787
Sandage A., 1987, AJ 93, 610
Soubiran C., 1993, A&A 274, 181
Spagna A., Lattanzi M.G., Lasker B.M., et al., 1996, A&A, 311, 758
Wielen R., Jahreiss H., Krüger R., 1983, In: Philip A.G.D., Upgren A.R. (eds.) The Nearby Stars and the Stellar Luminosity Function. IAU Coll. 76, L. Davis Press, Schenectady, p. 163